Cellular and Molecular Neurobiology (2019) 39:255–263
https://doi.org/10.1007/s10571-018-0645-y

ORIGINAL RESEARCH

Molecular Imaging of mGluR5 Availability with [^{11}C]ABP68 in Glutaminase Heterozygous Mice

Lauren Kosten[1] · Steven Deleye[1] · Sigrid Stroobants[1,4] · Leonie Wyffels[1,4] · Susana Mingote[2,3] · Stephen Rayport[2,3] · Steven Staelens[1]

Received: 23 August 2018 / Accepted: 10 December 2018 / Published online: 14 December 2018

Abstract

Many PET tracers enable determination of fluctuations in neurotransmitter release, yet glutamate specifically can not be visualized in a noninvasive manner. Several studies point to the possibility of visualizing fluctuations in glutamate release by changes in affinity of the mGluR5 radioligand [^{11}C]ABP688. These studies use pharmacological challenges to alter glutamate levels, and so probe release, but have not measured chronic alterations in receptor occupancy due to altered neurotransmission relevant to chronic neuropsychiatric disorders or their treatment. In this regard, the GLS1 heterozygous mouse has known reductions in activity of the glutamate-synthetic enzyme glutaminase, brain glutamate levels and release. We imaged this model to elucidate glutamatergic systems. Dynamic [^{11}C]ABP688 microPET scans were performed for mGluR5. Western blot was used as an ex vivo validation. No significant differences were found in BP_{ND} between WT and GLS1 Hets. SPM showed voxel-wise increased in BP_{ND} in GLS1 Hets compared to WT consistent with lower synaptic glutamate. This was not due to alterations in mGluR5 levels, as western blot results showed lower mGluR5 levels in GLS1 Hets. We conclude that because of the chronic glutaminase deficiency and subsequent decrease in glutamate, the mGluR5 protein levels are lowered. Due to these decreased endogenous glutamate levels, however, there is increased [^{11}C]ABP688 binding to the allosteric site in selected regions. We speculate that lower endogenous glutamate leads to less conformational change to the receptors, and thus higher availability of the binding site. The lower mGluR5 levels, however, lessen [^{11}C]ABP688 binding in GLS1 Hets, in part masking the increase in binding due to diminished endogenous glutamate levels as confirmed with voxel-wise analysis.

Keywords Glutamate · Micro PET · Glutaminase · Western blot · mGluR5

Abbreviations

[^{11}C]ABP688	3-(6-Methyl-pyridin-2-ylethynyl)-cyclohex-2-enone-*O*-[^{11}C]-methyl-oxime
BP_{ND}	Nondisplaceable binding potential
CB	Cerebellum
CT	Computed tomography
FOV	Field of view
GLS1	Glutaminase
HIP	Hippocampus
Het	Heterozygous
i.v.	Intravenous
MID	Midbrain
mPFC	Medial prefrontal cortex
mGluR5	Metabotropic glutamate receptor 5
NMDA	*N*-methyl-D-aspartate
PAG	Phosphate-activated glutaminase
PET	Positron emission tomography
SDS-PAGE	Sodium dodecyl sulfate polyacrylamide gel electrophoresis
SPM	Statistical parametric mapping
SRTM	Simplified reference tissue model
TAC	Time-activity curve
THA	Thalamus
VOI	Volume of interest
WT	Wild type

✉ Steven Staelens
steven.staelens@uantwerpen.be

[1] Molecular Imaging Center Antwerp, University of Antwerp, Antwerp, Belgium

[2] Department of Psychiatry, Columbia University, New York, USA

[3] Molecular Therapeutics, NYS Psychiatric Institute, New York, USA

[4] Department of Nuclear Medicine, University Hospital Antwerp, Antwerp, Belgium

Introduction

Imaging acute fluctuations in endogenous neurotransmitters has been a major development in the field of molecular imaging and has provided tools for the understanding of neurotransmitter alterations in several pathologies. Glutamate is the most abundant excitatory neurotransmitter. From a clinical standpoint, the search for glutamate imaging methods has its applications for studies regarding the involvement of glutamate synaptic mechanisms in the pathophysiology of various neurologic disorders and as potential therapeutic targets (Moghaddam and Javitt 2012).

The visualization of acute fluctuations in endogenous glutamate levels was first suggested by Miyake et al. in a PET study performed in baboons with the radioligand [^{11}C]ABP688 (3-(6-methyl-pyridin-2-ylethynyl)-cyclohex-2-enone-*O*-[^{11}C]-methyl-oxime), an allosteric antagonist for mGluR5. A significant decrease in tracer binding was reported after pharmacologic challenge with *N*-acetylcysteine (NAc), known to indirectly increase extrasynaptic glutamate release (Miyake et al. 2011). This study suggested that a glutamate receptor PET tracer could be used to measure changes in glutamate levels in vivo, assuming that the NAc-induced glutamate increase produced a shift in the binding affinity of the radioligand to an allosteric site of mGluR5. However, repeated studies in both rats (Wyckhuys et al. 2013) and Rhesus monkeys (Sandiego et al. 2013) were unable to replicate this finding with both NAc and MK801 as glutamate-increasing pharmacological challenges.

A 2015 study by Zimmer et al. first used ceftriaxone as a pharmacological challenge to decrease endogenous glutamate levels and found that this increased [^{11}C]ABP688 binding. It was argued by the authors that radioligand binding to the allosteric site is significantly variable based on the tertiary structure of the receptor and its interaction with other subunits to assume quaternary receptor conformations (Zimmer et al. 2015). Hence, glutamate levels may in fact alter mGluR5 conformational states. As quaternary structures, mGluR5 is known to assume monomeric or homodimeric forms, and there is even evidence for the existence of post-synaptic mGluR5/D_2R/A_{2A}R oligomers (Cabello et al. 2009) and pre-synaptic A_{2A}R/mGluR5 heterodimers modulating glutamate transmission (Rodrigues et al. 2005). Furthermore, there is knowledge of receptor regulatory proteins such as NECAB2 binding to mGluR5 to modulate receptor function (Canela et al. 2009). Not long afterward, the group of DeLorenzo revisited the effects of pharmacologically increased glutamate by infusing subjects continuously with ketamine (DeLorenzo et al. 2015). This study explored the hypothesis that glutamate release during ketamine infusion would reduce radioligand binding to mGluR5 through noncompetitive mechanisms. This study provided first evidence that ketamine administration decreases [^{11}C]ABP688 binding about 20% in vivo in human subjects. A finding that was replicated later in a study by Esterlis et al. and further linked to an antidepressant response to the ketamine administration (Esterlis et al. 2018). Both studies point to increased receptor internalization, reducing the ligand affinity. Esterlis et al. even point out that reductions in mGluR5 availability persisted for 24 h following ketamine administration. Our group tried to replicate the ketamine infusion studies by DeLorenzo's and Esterlis' group in rats. No significant differences were found due to the effects of ketamine, even though we effectively showed adequate ketamine levels were infused (Kosten et al. 2018). Though this study did not corroborate previous human studies (DeLorenzo et al. 2015; Zimmer et al. 2015), it did confirm in vivo results in anesthetized animals (Sandiego et al. 2013; Wyckhuys et al. 2013; Kosten et al. 2016). Both species differences and effects of anesthesia could hence dictate the difference in findings. Moreover, all of the previous work makes use of a pharmacological challenge, only being able to cause acute changes to endogenous glutamate levels, instead of a steady alteration.

A study by our group also explored the effect of repeated chronic MK801 challenges, as glutamate-increasing agent, over a period of 1 month to explore changes in mGluR5 availability (Kosten et al. 2016). No significant differences were found over different time points, though a trend in increased mGluR5 availability was seen despite extensive tissue loss caused by the chronic MK801 injections. Overall glutamate levels were in fact decreased through the chronic nature of the challenge as found earlier (Tsukada et al. 2005; Zuo et al. 2006) and is recently confirmed by another study by our group (Servaes et al. 2018).

Therefore, based on all the aforementioned work, we chose to further try to elucidate the glutamatergic system with the tools available and to alter glutamate levels chronically by genetic manipulation of a mouse model. Our hypothesis is that higher levels of endogenous glutamate lead to conformational changes to mGluR5, decreasing its availability to ligands, and therefore radioligands. Lower glutamate levels would provoke less conformational receptor changes, and therefore, the current expectation is that there will be more radioligand binding to mGluR5. Our target of interest to cause chronic glutamate decrease is the enzyme glutaminase.

The conversion of glutamine into glutamate is catalyzed by phosphate-activated glutaminase (PAG). Recently, glutaminase has been identified as a promising novel therapeutic target for the pharmacotherapy of schizophrenia (Gaisler-Salomon et al. 2009; El Hage et al. 2012; Mingote et al. 2016) with potential for obsessive compulsive disorder.

There are two genes encoding PAG. The first one (GLS1) codes for the form present in the brain and kidneys. The second one (GLS2) encodes the liver isoform. PAG has a crucial role in brain function, since full knockout of the GLS1 gene is neonatal lethal (Masson et al. 2006). The GLS1 heterozygous model is a resilience model (Gaisler-Salomon et al. 2009; Mingote et al. 2016) and therefore models potential therapeutic mechanisms rather than disease mechanisms (Gaisler-Salomon et al. 2012; Hazan and Gaisler-Salomon 2014; Mingote et al. 2016). GLS1 heterozygous mice display a cognitive phenotype with adult onset, reflecting both slightly reduced and enhanced cognition (Gaisler-Salomon et al. 2012; Mihali et al. 2012; Hazan and Gaisler-Salomon 2014).

The model of choice is GLS1 Het mice, originally developed to be stopGLS1 mice with a transcriptional block of GLS1 (Masson et al. 2006; El Hage et al. 2012; Mingote et al. 2016). GLS1 Hets are resilient to some of the propsychotic effects of ketamine and amphetamine. PAG activity is reduced by approximately 20% (Gaisler-Salomon et al. 2009; Moghaddam and Javitt 2012; El Hage et al. 2012; Mingote et al. 2016), and glutamate levels are decreased by approximately 15% (Gaisler-Salomon et al. 2009; Moghaddam and Javitt 2012). Figure 1 illustrates glutamine metabolism in the brain, indicating the steps in the pathway that are affected by GLS1 gene knockout.

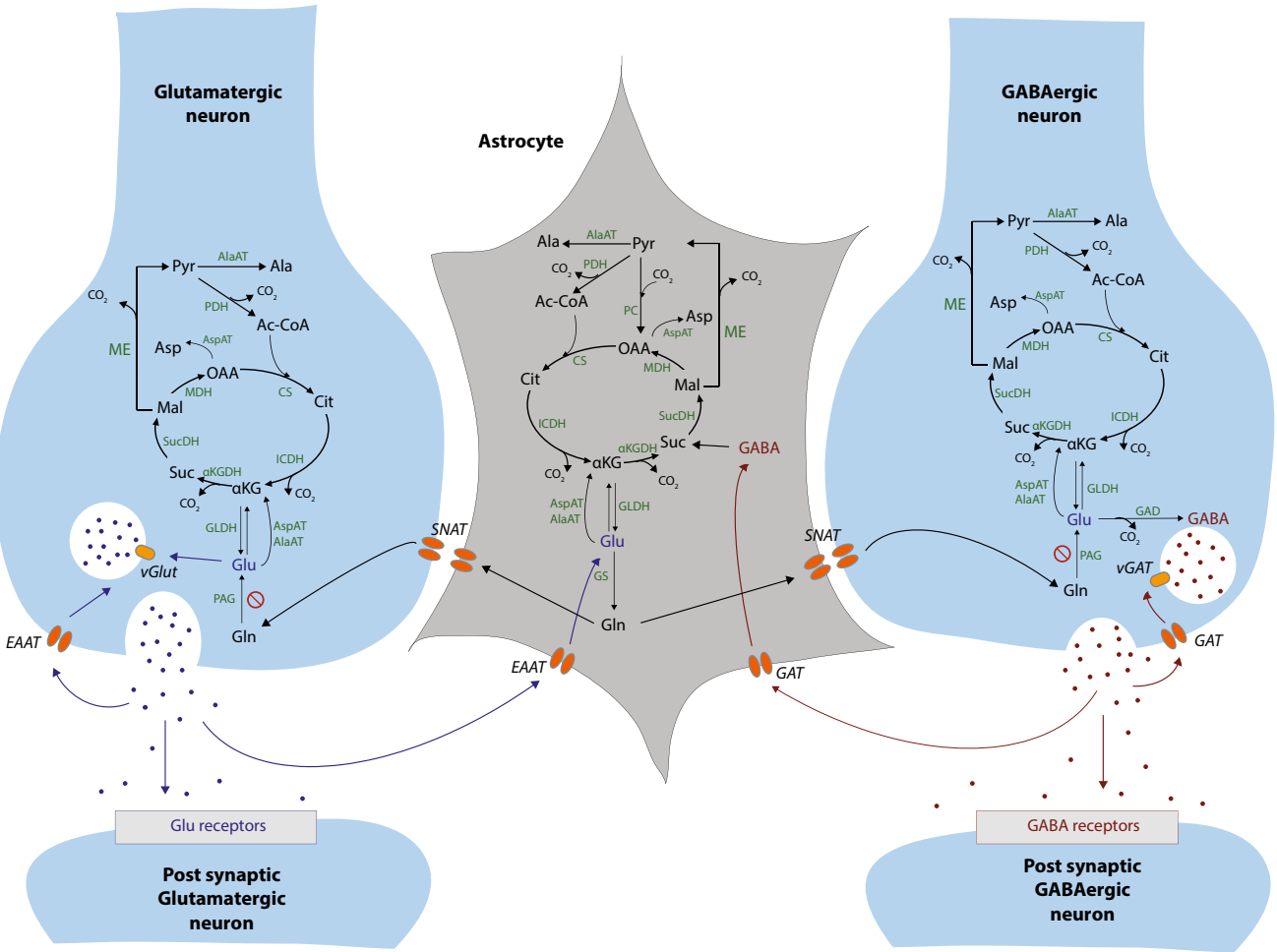

Fig. 1 Scheme of glutamine metabolism in the brain, inspired on El Hage et al. 2012. *PAG* phosphate-activated glutaminase, *GS* glutamine synthetase, *GLDH* glutamate dehydrogenase, *AlaAT* alanine aminotransferase, *AspAT* aspartate aminotransferase, *GAD* glutamic acid decarboxylase, *GABA-T* gamma aminobutyric acid aminotransferase, *aKGDH*, a-ketoglutarate dehydrogenase, *SucDH* succinate dehydrogenase, *MDH* malate dehydrogenase, *ME* malic enzyme, *PDH* pyruvate dehydrogenase, *PC* pyruvate carboxylase, *CS* citrate synthase, *ICDH* isocitrate dehydrogenase, *TCA cycle* tricarboxylic acid cycle, *Gln* glutamine, *Glu* glutamate, *aKG* a-ketoglutarate, *Suc* succinate, *Mal* malate, *OAA* oxaloacetate, *Cit* citrate, *Asp* aspartate, *Pyr* pyruvate, *Ala* alanine, *Ac-CoA* acetyl coenzyme A, *GABA* gamma-aminobutyric acid

Materials and Methods

Radiosynthesis

[^{11}C]ABP688 was prepared as previously published (Wyckhuys et al. 2013). [^{11}C]ABP688 is a noncompetitive and highly selective antagonist for mGluR5.

Animals

The following study was conducted with floxGLS1 mice (Gaisler-Salomon et al. 2009; Mingote et al. 2016) as opposed to stopGLS1 mice, bred with deleter mice to generate GLS1 Δ/+ mice, where GLS1 expression is blocked by deletion of the coding region of GLS1 exon 1, including the transcriptional start sequence. We used mice with 50:50 C57BL/6J:129J background by breeding GLS1 Δ/+ mice with WT mice to yield GLS1 Δ/+ experimental mice and WT litter-mate controls (IACUC Approval Protocol Number NYSPI-1428). Twenty-two animals were scanned in adulthood, subdivided in a WT cohort ($n=12$) and a GLS1 Δ/+ (GLS1 Het) cohort. Animals were 142.46 ± 10.10 days of age (weight 24.96 ± 4.91 g and 24.04 ± 4.21 g for WT and GLS1 Hets, respectively) at the time of scanning. The study protocol was approved by the local Animal Experimental Ethical Committee of the University of Antwerp, Belgium (ECD 2016-83). All scans and catheterizations were performed under isoflurane anesthesia, and all efforts were made to minimize animal suffering according to the European Committee Guidelines (decree 2010/63/CEE) and the Animal Welfare Act (7 USC 2131).

PET-Acquisitions

For optimal throughput, animals were positioned side-by-side in the field-of-view (FOV) on a Siemens Inveon PET-CT scanner (Siemens Preclinical Solution, Knoxville, TN, USA). Dynamic acquisitions were performed as illustrated in Fig. 2 through simultaneous tracer injection (injected dose 5401.31 ± 1141.92 kBq for WT and 5202.81 ± 1387.72 kBq for GLS1 Hets) with a pump (Pump 11 Elite Dual Syringe, Harvard Apparatus, Les Ulis Cedex, France) at start of the scan. For tracer injection, catheters were placed in the tail vein under 1.5% isoflurane gas anesthesia, before positioning on the scanner. The injected tracer volume was 0.2 mL.

Image Processing

Acquired data were histogrammed and reconstructed into 23 frames of increasing length (2×10 s, 3×20 s, 3×30 s, 3×60 s, 3×150 s and 9×300 s) using software provided by the scanner manufacturer (Siemens Inveon Acquisition Workplace version 2.0). In addition, a single static image, covering the full 60 min, was reconstructed from the same data. For quantitative analysis, these images were reconstructed using 4 iterations and 16 subsets of the 2D ordered subset expectation maximization (OSEM 2D) algorithm following Fourier rebinning (FORE). Normalization, dead time, random, CT-based attenuation and single-scatter simulation (SSS) scatter corrections were applied. PET image frames were reconstructed on a $128 \times 128 \times 159$ grid with $0.776 \times 0.776 \times 0.796$ mm.

All PET image data were processed and analyzed with PMOD 3.6 software (Pmod Technologies, Zurich, Switzerland) for any regional and voxel-based analysis. Spatial normalization of the PET/CT images was done through rigid body image co-registration of the static PET images to an in house developed [^{11}C]ABP-688 PET template. Dynamic PET images were then transformed according to the above matrix. Using the predefined volume-of-interest (VOI) template, time activity curves (TACs) of different regions were extracted from the images and were then fitted by a simplified reference tissue model (SRTM) (Lammertsma and Hume 1996) with the cerebellum as reference region to calculate the BP_{ND}. Individual BP_{ND} images were obtained, respectively, through the basis function implementation of the SRTM with a fixed k2′ (Wu and Carson 2002) also using the cerebellum as the reference region.

Further, we have analyzed the data with Statistical Parametric Mapping (SPM) using SPM12, a more sensitive voxel-based technique than averaged regional analysis. Before SPM analysis, BP_{ND} images were first smoothed using an isotropic Gaussian filter (FWHM = 0.5 mm). One-tailed t test between GLS1 Hets and WT mice were performed for each voxel.

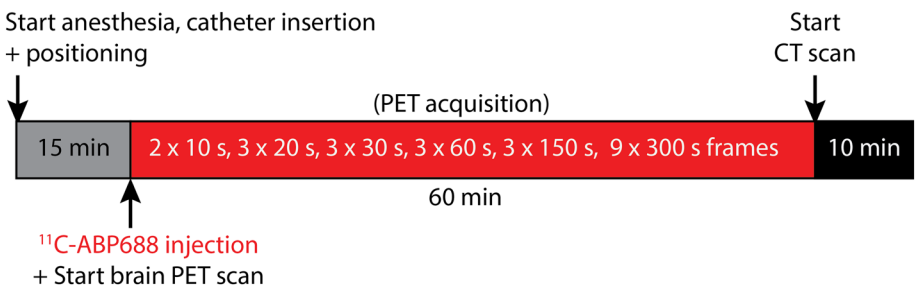

Fig. 2 Protocol of the [^{11}C] ABP688 scans for mGluR5

T-maps were thresholded at a significance level of 0.05 with a cluster extent threshold of 100 voxels (0.8 mm^3).

Western Blot

Brain regions were dissected from WT and GLS1 Het mice (Striatum, cerebellum, thalamus, cortex, midbrain, hippocampus and brain stem) and quickly frozen in isopentane in liquid nitrogen. Tissue was solubilized in RIPA lysis and extraction buffer (ThermoFisher Scientific, Gent, Belgium) supplement with protease inhibitors (Halt protease inhibitor cocktail, ThermoFisher Scientific), and the soluble lysate was sonicated and vortexed, before 15 min centrifugation at 4 °C and 14,000 rpm. After centrifugation, protein levels in the supernatant were measured using Pierce BCA kit (ThermoFisher Scientific) and 15 µg protein was taken for each sample. After addition of 4x Laemmli sample buffer (Bio-Rad, Temse, Belgium), samples were cooked on 100 °C for 6 min and kept on ice until loading on the 4–15% gradient SDS-PAGE gel (Mini-Protean TGX precast, Bio-Rad). SDS-PAGE was run at 100 V for 70 min, followed by protein transfer on PVDF membrane (Millipore, Overijse, Belgium) at 30 V overnight. Membrane was blocked with Odyssey blocking buffer 1:1 (Li-Cor, Leusden, The Netherlands) in TBS for 1 h. Membranes were immunoblotted with primary antibody for mGluR5 (1:1000 AB5675, Millipore) in 1:1 blocking buffer in TBS supplemented with 0.1% Tween, followed by 4 washes in TBS-T and secondary incubation with anti-rabbit IgG Alexa-488 (1:20,000, Li-Cor, Leusden, The Netherlands) in 1:1 blocking buffer in TBS supplemented with 0.1% Tween and 0.01% SDS. After 4 more washing steps with TBS-T followed by a washing step in TBS, blots were scanned with the Oddyssey imaging system (Li-cor). Subsequently the blot was stripped and reprobed for β-actin (mouse monoclonal anti-β-actin, Sigma-Aldrich, Dorset, UK) to ensure equal loading and transfer of proteins. All scanned blots were analyzed in ImageStudioLite v5.2.5 (Li-cor).

Statistical Analyses

Statistical significance was determined using the Holm–Sidak *t* test, with $\alpha = 5.000\%$ in GraphPad Prism 6.0 (GraphPad Software Inc, San Diego, CA, USA).

Each region was analyzed individually, without assuming a consistent SD.

Results

[^{11}C]ABP688 BP_{ND}

Figure 3 illustrates microPET images of BP_{ND} as an overlay on an MRI template used to determine the VOIs. No significant difference is found between GLS1 Hets and WT animals. BP_{ND} is 0.93 ± 0.14 and 0.99 ± 0.10 in the striatum for WT and GLS1 Hets, respectively. For the cortex, these values are 0.59 ± 0.09 and 0.64 ± 0.07, 0.74 ± 0.11 and 0.78 ± 0.13 in hippocampus, 0.27 ± 0.10 and 0.29 ± 0.13 for the midbrain, 0.55 ± 0.08 and 0.59 ± 0.07 in the thalamus and 0.39 ± 0.07 and 0.44 ± 0.06 in the hypothalamus for WT and GLS1 Het animals, respectively, as shown in Fig. 4. Other regions of interest are summarized in Table 1.

SPM

SPM voxel-based analysis, being statistically more sensitive than a VOI-based approach, showed that BP_{ND} in GLS1 Het animals is significantly higher than in WT throughout cerebellum, brain stem, midbrain and thalamus (Fig. 5). No voxels with significantly lower BP_{ND} in GLS1 Hets than WT were found.

mGluR5 Western Blot

As seen in the literature on altered expression of mGluR5 in various pathologies, mGluR5 protein can appear as monomers between 112 and 130 kDa, as well as in dimeric form of approximately 224–250 kDa on blots (Fatemi et al. 2011; Fatemi and Folsom 2014). To investigate protein levels in the brain of GLS1 Hets and WT mice, we performed immunoblotting for mGluR5 on dissected brain regions obtained after the PET scans as exemplified in Fig. 6a, resulting in the finding that total mGluR5 levels (monomeric and dimeric) tend to be lower ($p = 0.09$) in the thalamus as shown in Fig. 6c and significantly so in midbrain ($p = 0.006$) and hippocampus ($p = 0.03$) of GLS1 Het animals compared to WT mice, shown in Fig. 6b, d, respectively. The difference in other regions was not statistically significant. When looking solely at the more abundant monomeric form of mGluR5, as illustrated in Fig. 6a, the same conclusions can be made

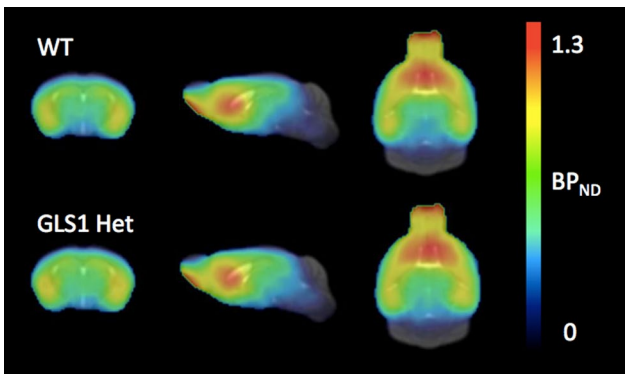

Fig. 3 Mean PET BP_{ND} images of the two conditions (WT and GLS1 Hets $n = 12$ and $n = 10$, respectively), overlaid on an MR template

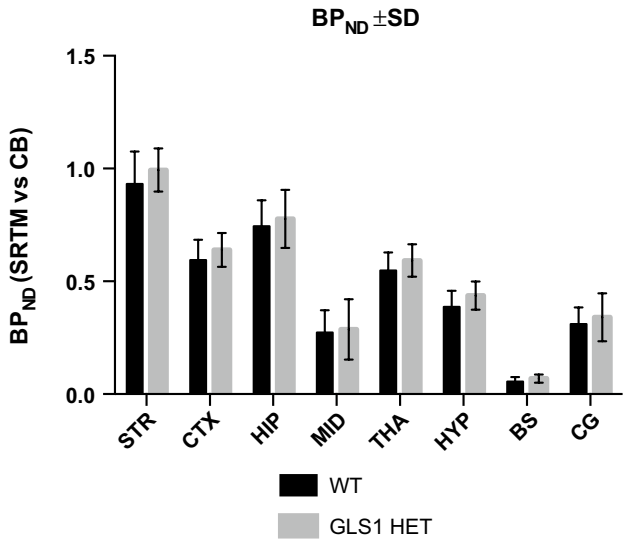

Fig. 4 Mean BP_{ND} values for the two conditions (WT and GLS1 Hets $n=12$ and $n=11$, respectively), in the delineated VOIs. Error bars represent SD with *STR* striatum, *CTX* cortex, *HIP* hippocampus, *MID* midbrain, *THA* thalamus, *HYP* hypothalamus, *BS* brain stem, *CG* cingulate cortex

Table 1 Mean BP_{ND} values for the two conditions (WT and GLS1 Hets $n=12$ and $n=11$, respectively), in the delineated VOIs

	WT		GLS1 Het		*t* test
	Mean	SD	Mean	SD	*p* value
STR	0.93	0.14	0.99	0.10	0.24
CTX	0.59	0.09	0.64	0.07	0.21
HIP	0.74	0.11	0.78	0.13	0.53
MID	0.27	0.10	0.29	0.13	0.81
THA	0.55	0.08	0.59	0.07	0.17
BFS	0.76	0.12	0.80	0.08	0.39
HYP	0.39	0.07	0.44	0.06	0.09
RAMY	0.63	0.12	0.68	0.13	0.69
LAMY	0.59	0.11	0.63	0.10	0.98
BS	0.06	0.02	0.07	0.02	0.18
CG	0.31	0.07	0.34	0.11	0.49
SC	0.51	0.10	0.55	0.10	0.34
OLF	0.71	0.15	0.71	0.07	0.93
LIC	0.33	0.07	0.34	0.07	0.61
RIC	0.32	0.06	0.37	0.08	0.10

regarding significance ($p<0.05$) in the above-mentioned regions. Dimer/monomer ratio for mGluR5 did not differ between groups.

Discussion

Previously, increases were found in mGluR5 visualized through immunohistochemistry in pharmacological models with lower glutamate levels (Kosten et al. 2016; Servaes et al. 2018). However, in this study with the GLS1 genetic mouse model, Western blot shows that mGluR5 protein levels tend to be lower in thalamus and are significantly declined in both hippocampus and midbrain in GLS1 Het mice. Indeed, with a genetically modified mouse, which has the glutaminase impairment from birth, an altered development of receptor levels was to be expected (Bae et al. 2013). As mGluR5 protein bands on western blot can appear as both monomeric and homodimeric form, we included all for calculations of total expression. Most occurring dimers, however, undergo denaturation during the process, hence the detection of most protein around 132 kDa. Alterations that were found in either isoform and total levels were similar, and no ratio differences were found.

No significant differences were found in BP_{ND} between WT and GLS1 Hets, despite a known decrease of 15% in glutamate levels in GLS1 Het mice. A more sensitive SPM analysis shows voxel-wise a higher BP_{ND} in GLS1 Hets versus WT in cerebellum, brain stem, midbrain and thalamus. This higher BP_{ND} in the presence of an actual decrease in mGluR5 protein expression might reflect that receptor availability to the radioligand is possibly even higher and slightly masked by the lower expression in the GLS1 Het model.

We argue that an increase in BP_{ND} for [^{11}C]ABP688 is compatible with a lower level of endogenic glutamate comparable to ceftriaxone administration in rats lowering extracellular glutamate levels and increasing [^{11}C]ABP688 binding (Zimmer et al. 2015). We know that glutamate is indeed decreased because of our animal model's properties (Gaisler-Salomon et al. 2009). Because of this chronically lowered glutamate level, we hypothesize that the receptors undergo less conformational changes, allowing [^{11}C]ABP688 to bind more, leading to an increased BP_{ND}. This corroborates the argument made by the group of DeLorenzo and Esterlis that surges in glutamate levels do lead to conformational changes of mGluR5, reducing the ability of the radioligand to bind (Esterlis et al. 2018). Moreover, one of our previously published studies following chronic MK801 and/or NAc administration in rats (Kosten et al. 2016) also shows an increasing trend in [^{11}C]ABP688 binding as endogenous glutamate levels in that study were in fact lowered due to the repeated injection paradigm (Tsukada et al. 2005; Zuo et al. 2006), which supports our current findings as well. The same conclusions were reconfirmed by another study from our group again applying repeated MK801 injections to rats in a 7 day protocol (Servaes et al. 2018). Our interpretation of how allosteric ligands such as

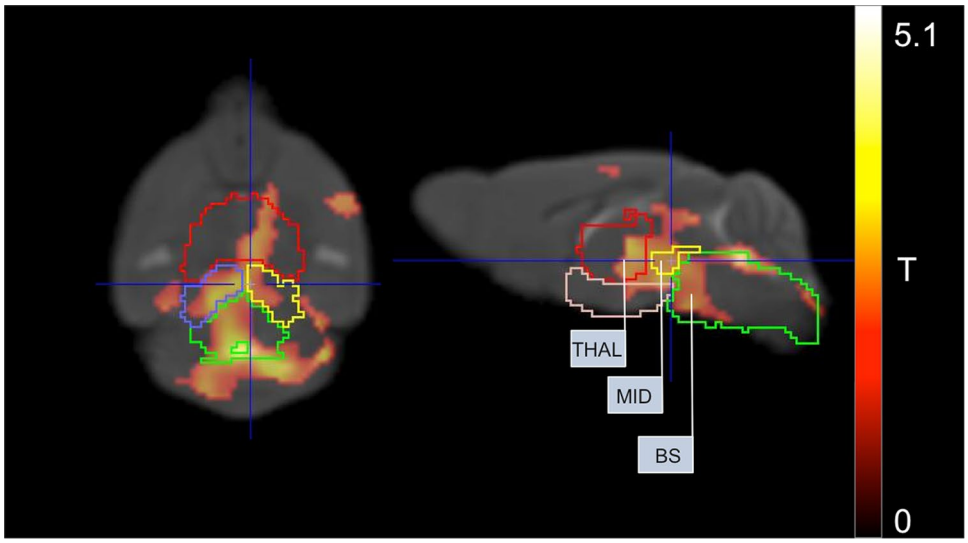

Fig. 5 T-maps (cluster size 100 voxels) showing higher BP_{ND} in GLS1 Het animals compared to WT in cerebellum, brain stem, midbrain and thalamus

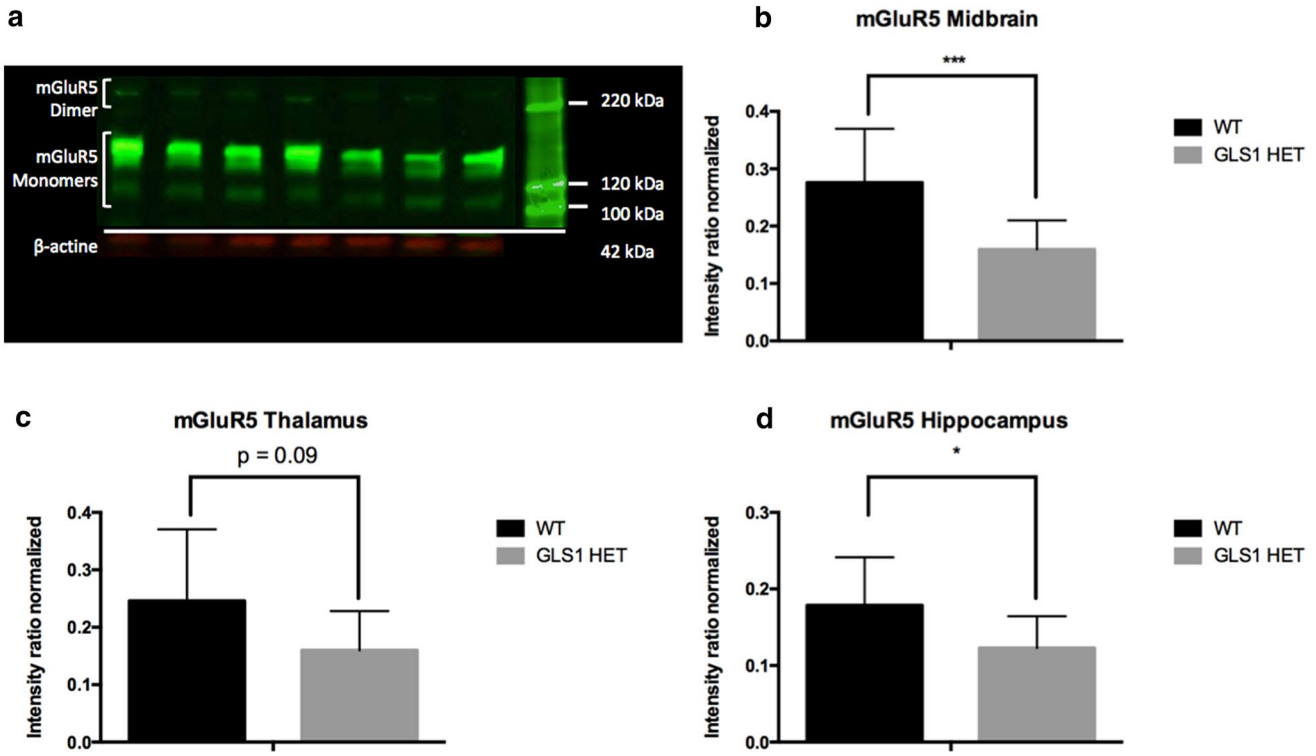

Fig. 6 **a** Representative sample of immunoblotting for mGluR5 and β-actin in mouse brain lysate from the PET scanned animals. mGluR5 was visible in both monomeric and dimeric form in all animals. β-actin immunostaining was used as a loading control. **b** Quantified mGluR5 density values corrected for loading control density for the two conditions (WT and GLS1 Hets $n=12$ and $n=11$, respectively) in midbrain with lower protein concentration ($p=0.006$) for GLS1 Hets compared to WT. **c** Quantified mGluR5 density values corrected for loading control density for the two conditions (WT and GLS1 Hets $n=12$ and $n=11$, respectively) in thalamus with lower protein concentration ($p=0.09$) for GLS1 Hets compared to WT. **d** Quantified mGluR5 density values corrected for loading control density for the two conditions (WT and GLS1 Hets $n=12$ and $n=11$, respectively) in Hippocampus with lower protein concentration ($p=0.03$) for GLS1 Hets compared to WT. Bars are displayed as mean + standard deviation

[^{11}C]ABP688 occupy the binding site remains speculative. Gregory et al. attempted to identify specific ligand–receptor interactions that govern binding to an mGluR5 allosteric site, their results highlighted the subtleties of allosteric binding to mGluR5 and a need for a deeper understanding of the specific ligand–receptor interactions (Gregory et al. 2014) .

All the previous taken together we confirm that chronic reductions in endogenous glutamate level increase [^{11}C]ABP688 radioligand binding to mGluR5.

The current main objective based on previous work was to continue efforts in elucidating [^{11}C]ABP688 in models of glutamate modulation. However, our results are relevant to the model which is proposed as a resilience model to schizophrenia, and as a future perspective to schizophrenia pathophysiology research. The model exhibits hippocampal hypoactivity (Gaisler-Salomon et al. 2012), making the altered protein expression in this region all the more relevant as both animal models of schizophrenia and patients have increased mGluR5 expression in this region (Matosin et al. 2015; Zurawek et al. 2017). The current findings seem to confirm a role for mGluR5 in the pathology.

Acknowledgements The collaboration with the Rayport laboratory at Columbia University was funded in part by FWO Grant V4.228.16N. We are grateful to Philippe Joye and Caroline Berghmans of MICA, University of Antwerp for their scan acquisitions, and to Christophe Deben and Annemie Van Eetveldt for their support setting up and executing the Western blot protocol.

Author Contributions LK, StSt and SR contributed to conceptualization and manuscript revision; LK, SR, SM, StSt and SD involved in methodology; LW contributed to resources; LK and SD executed formal analysis; LK and StSt were involved in investigation; LK wrote original draft; StSt and SS contributed to supervision.

Compliance with Ethical Standards

Conflict of interest The authors declare that they have no conflict of interest.

References

Bae N, Wang Y, Li L et al (2013) Network of brain protein level changes in glutaminase deficient fetal mice. J Proteom 80:236–249. https://doi.org/10.1016/j.jprot.2013.01.013

Cabello N, Gandía J, Bertarelli DCG et al (2009) Metabotropic glutamate type 5, dopamine D2 and adenosine A2a receptors form higher-order oligomers in living cells. J Neurochem 109:1497–1507. https://doi.org/10.1111/j.1471-4159.2009.06078.x

Canela L, Fernández-Dueñas V, Albergaria C et al (2009) The association of metabotropic glutamate receptor type 5 with the neuronal Ca^{2+}-binding protein 2 modulates receptor function. J Neurochem 111:555–567. https://doi.org/10.1111/j.1471-4159.2009.06348.x

DeLorenzo C, DellaGioia N, bloch M et al (2015) In vivo ketamine-induced changes in [(11)C]ABP688 binding to metabotropic glutamate receptor subtype 5. Biol Psychiatry 77:266–275. https://doi.org/10.1016/j.biopsych.2014.06.024

El Hage M, Masson J, Conjard-Duplany A et al (2012) Brain slices from glutaminase-deficient mice metabolize less glutamine: a cellular metabolomic study with carbon 13 NMR. J Cereb Blood Flow Metab 32:816–824. https://doi.org/10.1038/jcbfm.2012.22

Esterlis I, DellaGioia N, Pietrzak RH et al (2018) Ketamine-induced reduction in mGluR5 availability is associated with an antidepressant response: an [(11)C]ABP688 and PET imaging study in depression. Mol Psychiatry 23:824–832. https://doi.org/10.1038/mp.2017.58

Fatemi SH, Folsom TD (2014) Existence of monomer and dimer forms of mGluR5, under reducing conditions in studies of postmortem brain in various psychiatric disorders. Schizophr Res 158:270–271. https://doi.org/10.1016/j.schres.2014.06.029

Fatemi SH, Folsom TD, Kneeland RE, Liesch SB (2011) Metabotropic glutamate receptor 5 upregulation in children with autism is associated with underexpression of both Fragile X mental retardation protein and GABAA receptor beta 3 in adults with autism. Anat Rec (Hoboken) 294:1635–1645. https://doi.org/10.1002/ar.21299

Gaisler-Salomon I, Miller GM, Chuhma N et al (2009) Glutaminase-deficient mice display hippocampal hypoactivity, insensitivity to pro-psychotic drugs and potentiated latent inhibition: relevance to schizophrenia. Neuropsychopharmacology 34:2305–2322. https://doi.org/10.1038/npp.2009.58

Gaisler-Salomon I, Wang Y, Chuhma N et al (2012) Synaptic underpinnings of altered hippocampal function in glutaminase-deficient mice during maturation. Hippocampus 22:1027–1039. https://doi.org/10.1002/hipo.22014

Gregory KJ, Nguyen ED, Malosh C et al (2014) Identification of specific ligand–receptor interactions that govern binding and cooperativity of diverse modulators to a common metabotropic glutamate receptor 5 allosteric site. ACS Chem Neurosci 5:282–295. https://doi.org/10.1021/cn400225x

Hazan L, Gaisler-Salomon I (2014) Glutaminase1 heterozygous mice show enhanced trace fear conditioning and Arc/Arg3.1 expression in hippocampus and cingulate cortex. Eur Neuropsychopharmacol 24:1916–1924. https://doi.org/10.1016/j.euroneuro.2014.10.003

Kosten L, Verhaeghe J, Verkerk R et al (2016) Multiprobe molecular imaging of an NMDA receptor hypofunction rat model for glutamatergic dysfunction. Psychiatry Res 248:1–11

Kosten L, Verhaeghe J, Wyffels L et al (2018) Acute ketamine infusion in rat does not affect in vivo [^{11}C]ABP688 binding to metabotropic glutamate receptor subtype 5. Mol Imaging 17:1–5. https://doi.org/10.1177/1536012118788636

Lammertsma AA, Hume SP (1996) Simplified reference tissue model for PET receptor studies. NeuroImage 4:153–158. https://doi.org/10.1006/nimg.1996.0066

Masson J, Darmon M, Conjard A et al (2006) Mice lacking brain/kidney phosphate-activated glutaminase have impaired glutamatergic synaptic transmission, altered breathing, disorganized goal-directed behavior and die shortly after birth. J Neurosci 26:4660–4671. https://doi.org/10.1523/JNEUROSCI.4241-05.2006

Matosin N, Fernandez-Enright F, Fung SJ et al (2015) Alterations of mGluR5 and its endogenous regulators Norbin, Tamalin and Preso1 in schizophrenia: towards a model of mGluR5 dysregulation. Acta Neuropathol 130:119–129. https://doi.org/10.1007/s00401-015-1411-6

Mihali A, Subramani S, Kaunitz G et al (2012) Modeling resilience to schizophrenia in genetically modified mice: a novel approach to drug discovery. Expert Rev Neurother 12:785–799. https://doi.org/10.1586/ern.12.60

Mingote S, Masson J, Gellman C et al (2016) Genetic pharmacotherapy as an early CNS drug development strategy: testing glutaminase inhibition for schizophrenia treatment in adult mice. Front Syst Neurosci 9:1–12. https://doi.org/10.3389/fnsys.2015.00165

Miyake N, Skinbjerg M, Easwaramoorthy B et al (2011) Imaging changes in glutamate transmission in vivo with the metabotropic glutamate receptor 5 tracer [^{11}C] ABP688 and *N*-acetylcysteine challenge. Biol Psychiatry 69:822–824. https://doi.org/10.1016/j.biopsych.2010.12.023

Moghaddam B, Javitt D (2012) From revolution to evolution: the glutamate hypothesis of schizophrenia and its implication for treatment.

Neuropsychopharmacology 37:4–15. https://doi.org/10.1038/npp.2011.181

Rodrigues RJ, Alfaro TM, Rebola N et al (2005) Co-localization and functional interaction between adenosine A(2A) and metabotropic group 5 receptors in glutamatergic nerve terminals of the rat striatum. J Neurochem 92:433–441. https://doi.org/10.1111/j.1471-4159.2004.02887.x

Sandiego CM, Nabulsi N, Lin S-F et al (2013) Studies of the metabotropic glutamate receptor 5 radioligand [^{11}C]ABP688 with *N*-acetylcysteine challenge in rhesus monkeys. Synapse 67:489–501. https://doi.org/10.1002/syn.21656

Servaes S, Kara F, Glorie D et al (2018) In vivo molecular imaging of repeated exposure to an NMDA antagonist and a glutaminase inhibitor as potential glutamatergic modulators. J Pharmacol Exp Ther (**Accepted**)

Tsukada H, Nishiyama S, Fukumoto D et al (2005) Chronic NMDA antagonism impairs working memory, decreases extracellular dopamine, and increases D1 receptor binding in prefrontal cortex of conscious monkeys. Neuropsychopharmacology 30:1861–1869. https://doi.org/10.1038/sj.npp.1300732

Wu Y, Carson RE (2002) Noise reduction in the simplified reference tissue model for neuroreceptor functional imaging. J Cereb Blood Flow Metab 22:1440–1452. https://doi.org/10.1097/01.WCB.0000033967.83623.34

Wyckhuys T, Verhaeghe J, Wyffels L et al (2013) N-acetylcysteine- and MK-801-induced changes in glutamate levels do not affect in vivo binding of metabotropic glutamate 5 receptor radioligand ^{11}C-ABP688 in rat brain. J Nucl Med. https://doi.org/10.2967/jnumed.113.121608

Zimmer ER, Parent MJ, Leuzy A et al (2015) Imaging in vivo glutamate fluctuations with [(11)C]ABP688: a GLT-1 challenge with ceftriaxone. J Cereb Blood Flow Metab. https://doi.org/10.1038/jcbfm.2015.35

Zuo D-Y, Zhang Y-H, Cao Y et al (2006) Effect of acute and chronic MK-801 administration on extracellular glutamate and ascorbic acid release in the prefrontal cortex of freely moving mice on line with open-field behavior. Life Sci 78:2172–2178. https://doi.org/10.1016/j.lfs.2005.09.022

Zurawek D, Salerno-Kochan A, Dziedzicka-Wasylewska M et al (2017) Changes in the expression of metabotropic glutamate receptor 5 (mGluR5) in a ketamine-based animal model of schizophrenia. Schizophr Res. https://doi.org/10.1016/j.schres.2017.04.014